Available online at www.sciencedirect.com
SCIENCE DIRECT®
PERGAMON
Polyhedron 22 (2003) 2847–2854
POLYHEDRON
www.elsevier.com/locate/poly

Synthesis and structural characterization of $[H_xCp^*TiMo_5O_{18}]^{(3-x)-}$ ($x = 0, 1, 2$); new insights into protonation patterns in polyoxometalates

H. Akashi [a], J. Chen [b], H. Hasegawa [c], M. Hashimoto [d], T. Hashimoto [c], T. Sakuraba [c], A. Yagasaki [c,*]

[a] *Analysis Center, Okayama University of Science, Ridai-cho, Okayama 700, Japan*
[b] *Department of Chemistry, University of Illinois, Urbana, IL 61801, USA*
[c] *Department of Chemistry, Kwansei Gakuin University, Uegahara, Nishinomiya 662-8501, Japan*
[d] *Department of Material Science and Chemistry, Faculty of Systems Engineering, Wakayama University, Wakayama 640-8510, Japan*

Received 10 April 2003; accepted 27 June 2003

Abstract

Reaction of $[(n\text{-}C_4H_9)_4N]_2[Mo_2O_7]$, Cp^*TiCl_3, and $(n\text{-}C_4H_9)_4NOH$ in CH_3CN yields $[(n\text{-}C_4H_9)_4N]_3[Cp^*TiMo_5O_{18}]\cdot CH_3CN$ [$a = 12.863(4)$ Å, $b = 26.608(6)$ Å, $c = 24.534(4)$ Å, $\beta = 103.88(2)^\circ$, $Z = 4$, space group $P2_1/c$ (no. 14)]. Similar reaction without $(n\text{-}C_4H_9)_4NOH$ yields monoprotonated complex $[(n\text{-}C_4H_9)_4N]_2[HCp^*TiMo_5O_{18}]$, where, according to a single-crystal X-ray diffraction study [$a = 19.9550(4)$ Å, $b = 25.5420(8)$ Å, $c = 11.8820(3)$ Å, $\beta = 100.31(2)^\circ$, $Z = 4$, space group $P2_1/n$ (no. 14)], the anion is protonated at one of OMo_2 doubly-bridging oxygens. Reaction of $[(n\text{-}C_4H_9)_4N]_2[HCp^*TiMo_5O_{18}]$ with CCl_3COOH in $CHCl_3$ followed by crystallization from CH_3CN/Et_2O yields diprotonated $[(n\text{-}C_4H_9)_4N][H_2Cp^*TiMo_5O_{18}]\cdot 1/4(C_2H_5)_2O$, which, according to a single-crystal X-ray diffraction study [$a = 12.319(2)$ Å, $b = 16.105(3)$ Å, $c = 12.001(2)$ Å, $\alpha = 110.74(1)^\circ$, $\beta = 100.31(2)^\circ$, $\gamma = 82.777(5)$, $Z = 2$, space group $P\bar{1}$ (no. 2)], contains hydrogen-bonded dimers of $[H_2Cp^*TiMo_5O_{18}]^-$ ions. The $[Cp^*TiMo_5O_{18}]^{3-}$ is basic enough to form stable organometallic adducts like $[(\eta\text{-}C_8H_{12})Ir(Cp^*TiMo_5O_{18})]^{2-}$ and $[(\eta\text{-}C_8H_{14})Rh(Cp^*TiMo_5O_{18})]^{2-}$.

Keywords: Polyoxometalate; Protonation; Molybdenum; Molecular oxide

1. Introduction

Substitution of hexavalent metal centers with one or more lower valent metals has now become a more or less standard technique for obtaining polyoxometalates of higher basicity and reactivity [1–5]. Simple electronic argument predicts that the oxygen atoms bonded to those lower valent metals would be the most basic ones in the resulted structure [1,2]. An X-ray crystallographic study of $[CpTiW_5O_{18}]^{3-}$ and their conjugate acids supports this prediction [6]. The study revealed that oxygens that bridge Ti and W atoms are protonated in both $[HCpTiW_5O_{18}]^{2-}$ and $[H_2CpTiW_5O_{18}]^-$. However, this remains to be the only systematic structural study that addressed the basicity of the surface oxygens of activated polyoxoanions. The most basic sites of other examples are just inferred from the result of this study and the electrostatic argument. Not even the protonation site of the closely related $[CpTiMo_5O_{18}]^{3-}$ has been determined due to its instability against Brønsted acids and hydrolysis [7].

Previously we found that the protonation site of the $[Cp^*TiMo_5O_{18}]^{3-}$ anion, a more stable analogue of $[CpTiMo_5O_{18}]^{3-}$, is different from that of $[CpTiW_5O_{18}]^{3-}$ [8]. In $[HCp^*TiMo_5O_{18}]^{2-}$ the proton is attached to an oxygen atom that bridges two Mo atoms, not to the oxygen that connects Ti and Mo. This unexpected finding prompted us to synthesize the diprotonated anion $[H_2Cp^*TiMo_5O_{18}]^-$ and carry out

* Corresponding author. Tel.: +81-79-565-9077; fax: +81-79-565-8396.
E-mail address: yagasaki@kwansei.ac.jp (A. Yagasaki).

0277-5387/03/$ - see front matter © 2003 Elsevier Ltd. All rights reserved.
doi:10.1016/S0277-5387(03)00411-X

a full structural study of the series $[Cp^*TiMo_5O_{18}]^{3-}$, $[HCp^*TiMo_5O_{18}]^{2-}$, and $[H_2Cp^*TiMo_5O_{18}]^{-}$. Here we report the results.

2. Experimental

2.1. Reagents, solvents, and general procedures

The following were purchased from commercial sources and used without further purification: Cp^*TiCl_3 (Strem), P_2O_5, and acetone (Kishida), 10% ^{17}O-enriched water (Cambridge Isotope Laboratories), and 10% methanolic $(n\text{-}C_4H_9)_4NOH$ (Kanto). $[(n\text{-}C_4H_9)_4N]_2[Mo_2O_7]$, $[(\eta\text{-}C_8H_{12})Ir(CH_3CN)_2]PF_6$, $[(\eta\text{-}C_8H_{14})Rh(CH_3CN)_2]PF_6$, and $[(\eta\text{-}C_4H_7)_2Rh(CH_3CN)_2]PF_6$ were prepared according to literature procedures [9,10]. Reactions were handled under dry N_2 atmosphere using standard Schlenk technique unless otherwise stated.

2.2. Analytical procedures

Elemental analyses were performed by Toray Research Center, Shiga, Japan. Infrared spectra were recorded from mineral oil (Nujol) mulls between KBr plates on a Hitachi I-3000 spectrometer. Absorptions are described as follows: strong (s), medium (m), weak (w), and shoulder (sh). ^1H NMR spectra were recorded on a Varian Unity-Plus 300 (300 MHz) spectrometer and referenced against TMS. All the spectra described below displayed ^1H NMR resonances for the $[(n\text{-}C_4H_9)_4N]^+$ cation at δ 3.11 (m, NCH_2), 1.62 (m, $NCH_2CH_2CH_2CH_3$), 1.37 (m, $NCH_2CH_2CH_2CH_3$), and 0.97 (m, CH_3). ^{17}O NMR spectra were measured at 40.68 MHz on the same instrument and referenced externally to fresh tap water.

2.3. Synthesis of $[(n\text{-}C_4H_9)_4N]_3[Cp^*TiMo_5O_{18}]$

To a solution of $[(n\text{-}C_4H_9)_4N]_2[Mo_2O_7]$ (4.5 g, 5.7 mmol) in 35 ml of CH_3CN was added 7.0 ml of 10% methanolic solution of $(n\text{-}C_4H_9)_4NOH$ (2.3 mmol) with stirring. The mixed solution was stirred for 30 min before it was evaporated in vacuo. The resulting white sticky solid was redissolved in 35 ml of CH_3CN, and a solution of Cp^*TiCl_3 (0.70 g, 2.4 mmol, in 40 ml of CH_3CN) was added to this solution with stirring. The volume of the orange solution thus obtained was reduced to 1/3 under vacuum after it was stirred for 3 h. The yellow precipitate that formed on addition of 200 ml of diethyl ether to this solution was collected by filtration, washed with 2×10 ml of diethyl ether, and dried in vacuo for 3 h to yield 3.0 g of the product (1.8 mmol, 74% based on Ti). *Anal*. Calc. for $C_{58}H_{123}Mo_5N_3O_{18}Ti$: C, 41.5; H, 7.4; Mo, 28.6; N, 2.5; Ti, 2.9. Found: C, 41.3; H, 7.6; Mo, 28.2; N, 2.4; Ti, 2.8%. IR (Nujol, 1000–400 cm^{-1}): 916 (s), 880 (sh), 788 (s), 722 (sh), 678 (w), 666 (w), 556 (w), 480 (w). ^1H NMR (CD_3CN): δ 1.86 (Cp^*). ^{17}O NMR (CH_3CN): δ 859 (OMo, 4), 832 (OMo, 1), 649 (OTiMo, 4), 537 (OMo_2, 4), 515 (OMo_2, 4), −10 ($OTiMo_5$, 1).

^{17}O-Enriched material was prepared by dissolving 0.12 g (0.070 mmol) of $[(n\text{-}C_4H_9)_4N]_3[Cp^*TiMo_5O_{18}]$ in 1 ml of CH_3CN, adding 10 μl of 10% ^{17}O-enriched water, stirring the solution for 1 h, adding 40 ml of diethyl ether, collecting the yellow precipitate then formed by filtration, washing it with 2×2 ml of diethyl ether, and drying under vacuum for 6 h. Single crystals suitable for X-ray diffraction study were prepared by dissolving 0.36 g (0.21 mmol) of the product in 2.5 ml of CH_3CN and diffusing diethyl ether into the solution, redissolving 0.25 g of the needle-like crystals thus obtained in 2 ml of CH_3CN, adding diethyl ether to the point of saturation (1.7 ml), heating the mixture to obtain a clear solution, and then allowing the solution to stand at ambient temperature. Yellow plate-shaped crystals of $[(n\text{-}C_4H_9)_4N]_3[Cp^*TiMo_5O_{18}]\cdot CH_3CN$ appeared next day.

2.4. Synthesis of $[(n\text{-}C_4H_9)_4N]_2[HCp^*TiMo_5O_{18}]$

To a solution of $[(n\text{-}C_4H_9)_4N]_2[Mo_2O_7]$ (4.5 g, 5.7 mmol) in 100 ml acetone was added a solution of Cp^*TiCl_3 (0.70 g, 2.4 mmol, in 30 ml of acetone) and the mixed solution was stirred for 12 h. The solution was filtered to remove small amount of precipitate before it was evaporated to dryness under reduced pressure. The solid thus obtained was dissolved in 50 ml of $CHCl_3$, filtered to remove small amount of insoluble material. To this filtrate 25 ml of diethyl ether was added and the mixture was allowed to stand at ambient temperature for 2 days. The orange crystals then formed were collected by filtration, washed with 2×5 ml of diethyl ether, and dried in vacuo for 3 h to yield 1.8 g (1.3 mmol, 52% based on Ti) of the product. *Anal*. Calc. for $C_{42}H_{88}Mo_5N_2O_{18}Ti$: C, 35.1; H, 6.2; Mo, 33.4; N, 1.9; Ti, 3.3. Found: C, 34.7; H, 6.7; Mo, 33.3; N, 2.0; Ti, 3.3%. IR (Nujol, 1000–400 cm^{-1}): 964 (sh), 938 (s), 892 (m), 814 (s), 760 (sh), 634 (w), 610 (w), 544 (w), 476 (w). ^1H NMR (CD_3CN): δ 1.96 (Cp^*). ^{17}O NMR (CH_3CN): δ 897 (OMo, 5), 669 (OTiMo, 4), 544 (OMo_2, 8), −4 ($OTiMo_5$, 1).

^{17}O-Enriched material was prepared by dissolving 0.50 g (0.35 mmol) of $[(n\text{-}C_4H_9)_4N]_2[HCp^*TiMo_5O_{18}]$ in 3 ml of CH_3CN, adding 50 μl of 10% ^{17}O-enriched water, stirring the solution for 1 h, adding 60 ml of diethyl ether, collecting the orange precipitate then formed by filtration, washing it with 2×5 ml of diethyl ether, and drying under vacuum for 6 h.

2.5. Synthesis of $[(n\text{-}C_4H_9)_4N][H_2Cp^*TiMo_5O_{18}]$

To a solution of $[(n\text{-}C_4H_9)_4N]_2[HCp^*TiMo_5O_{18}]$ (0.35 g, 0.24 mmol, in 20 ml of $CHCl_3$) was added a solution of CCl_3COOH (0.10 g, 0.61 mmol, in $CHCl_3$) with stirring. The mixture was stirred for 15 min. The red precipitate that formed was collected by filtration, washed 2×2 ml of $CHCl_3$, and dried under vacuum to yield 0.25 g of the product (0.21 mmol, 86% yield). *Anal*. Calc. for $C_{26}H_{53}Mo_5NO_{18}Ti$: C, 26.1; H, 4.5; N, 1.2. Found: C, 26.1; H, 4.5; N, 1.2%. IR (Nujol, 1000–400 cm^{-1}): 978 (sh), 962 (s), 948 (sh), 928 (sh), 896 (w), 828 (s), 748 (m), 660 (m), 546 (w), 462 (2). ^1H NMR (CD_3CN): δ 2.06 (Cp*).

2.6. Synthesis of $[(n\text{-}C_4H_9)_4N]_2[(\eta\text{-}C_8H_{12})Ir(Cp^*TiMo_5O_{18})]$

In 20 ml of tetrahydrofuran were dissolved $[(n\text{-}C_4H_9)_4N]_3[Cp^*TiMo_5O_{18}]$ (0.80 g, 0.48 mmol) and $[(\eta\text{-}C_8H_{12})Ir(CH_3CN)_2]PF_6$ (0.25 g, 0.47 mmol). The reaction mixture was stirred for 10 min. The precipitate that formed on adding 60 ml of Et_2O to this solution was collected by filtration, washed with 2×10 ml of Et_2O, and then dried in vacuo. The crude product thus obtained was redissolved in 24 ml of tetrahydrofuran. Addition of 40 ml of Et_2O to this solution yielded crystalline, analytically pure material, which was collected by filtration, washed with 2×10 ml of Et_2O, and dried in vacuo (0.69 g, 0.40 mmol, 84% yield based on Ir). *Anal*. Calc. for $C_{50}H_{99}IrMo_5N_2O_{18}Ti$: C, 34.6; H, 5.7; Ir, 11.1; Mo, 27.6; N, 1.6; Ti, 2.8. Found: C, 34.8; H, 5.9; Ir, 10.9; Mo, 27.8; N, 1.6; Ti, 2.7%.

2.7. Synthesis of $[(n\text{-}C_4H_9)_4N]_2[(\eta\text{-}C_8H_{14})Rh(Cp^*TiMo_5O_{18})]$

In 5.0 ml of tetrahydrofuran were dissolved $[(n\text{-}C_4H_9)_4N]_3[Cp^*TiMo_5O_{18}]$ (0.19 g, 0.11 mmol) and $[(\eta\text{-}C_8H_{14})Rh(CH_3CN)_2]PF_6$ (0.04 g, 0.09 mmol). The dark brown solution was stirred for 1 h before 20 ml of Et_2O was added with stirring. The mixture was left stirred for another 30 min. Rust-colored precipitate that formed was collected by filtration, washed with 2×2 ml of Et_2O, and then dried in vacuo for 6 h to yield 0.11 g of the product (0.067 mmol, 73% on Rh). IR (Nujol, 1000–400 cm^{-1}): 934 (s), 880 (w), 808 (s), 788 (sh), 748 (m), 660 (w), 558 (w), 490 (w), 410 (m). ^1H NMR (CD_3CN): δ 0.98 (t, 24H), 1.37 (m, 18H), 1.61 (m, 22H), 1.92 (s, 15H), 2.09 (m, 2H), 3.11 (m, 18H), 3.25 (br, 2H) [11]. ^{17}O NMR (CH_3CN): δ 888 (OMo, 4), 881 (OMo, 1), 673 (OTiMo, 2), 667 (OTiMo, 2), 540 (OMo_2, 2), 532 (OMo_2, 2), 415 ($ORhMo_2$, 1), 294 ($ORhMo_2$, 2), −8 ($OTiMo_5$, 1).

2.8. Crystal structure determination

A yellow plate-like crystal of $[(n\text{-}C_4H_9)_4N]_3[Cp^*TiMo_5O_{18}]\cdot CH_3CN$ (**A**) with approximate dimensions $0.35 \times 0.20 \times 0.20$ mm was mounted on a grass capillary and coated with epoxy resin. A yellow plate-like crystal of $[(n\text{-}C_4H_9)_4N]_2[HCp^*TiMo_5O_{18}]$ (**B**) having approximate dimensions of $0.20 \times 0.15 \times 0.15$ mm was sealed in a glass capillary. An orange prism crystal of $[(n\text{-}C_4H_9)_4N][H_2Cp^*TiMo_5O_{18}]$ $1/4(C_2H_5)_2O$ (**C**) having approximate dimensions of $0.15 \times 0.10 \times 0.03$ mm was mounted in a loop. The diffraction data were collected on a RIGAKU AFC5R automated four-circle diffractometer (**A**), Mac Science MXC-18 diffractometer (**B**), or Rigaku/MSC Mercury diffractometer (**C**) using graphite monochromated Mo Kα radiation. The structures were solved by the Patterson and direct methods (**A**) or by the direct method (**B** and **C**). All structures were refined by the full-matrix least-squares method. The TEXSAN crystallographic software package [12] was used for **B** and **C**. The structure of **A** was solved and refined using the SHELX-97 program [13] after the initial data processing with TEXSAN. Crystallographic data are summarized in Table 1. Selected interatomic distances for the $[Cp^*TiMo_5O_{18}]^{3-}$, $[HCp^*TiMo_5O_{18}]^{2-}$, and $[H_2Cp^*TiMo_5O_{18}]^{-}$ anions are listed in Table 2 together with those for the Cp analogue. Table 3 gives C_{4v}-averaged distances for each anions.

3. Results and discussion

3.1. Synthesis and characterization

The compound $[Cp^*TiMo_5O_{18}]^{3-}$ is prepared in CH_3CN as a tetrabutylammonium salt according to Eq. (1).

$$5[Mo_2O_7]^{2} + 2Cp^*TiCl_3 + 2OH^- \rightarrow 2[Cp^*TiMo_5O_{18}]^{3-} + 6Cl^- + H_2O \quad (1)$$

Its IR spectrum is extremely similar to those of the Cp and W analogues, $[CpTiMo_5O_{18}]^{3-}$ [1], $[CpTiW_5O_{18}]^{3-}$ [1,3], and $[Cp^*TiW_5O_{18}]^{3-}$ [3,14] suggesting the same basic metal–oxygen framework (see Section 2). This has been confirmed by a single-crystal X-ray diffraction study (see below). The new anion, on the other hand, is more stable than the Cp analogue, $[CpTiMo_5O_{18}]^{3-}$. It does not decompose in the presence of a strong acid like HCl or CCl_3COOH, while $[CpTiMo_5O_{18}]^{3-}$ decomposes readily under similar conditions [4]. Also it has a higher basicity than the W analogues, $[CpTiW_5O_{18}]^{3-}$ and $[Cp^*TiW_5O_{18}]^{3-}$. The current anion undergoes spontaneous protonation in moist $CHCl_3$, while the W analogues are not protonated under similar conditions.

Table 1
Crystallographic data for $[(n\text{-}C_4H_9)_4N]_3[Cp^*TiMo_5O_{18}]\cdot CH_3CN$ (**A**), $[(n\text{-}C_4H_9)_4N]_2[HCp^*TiMo_5O_{18}]$ (**B**), and $[(n\text{-}C_4H_9)_4N][H_2Cp^*TiMo_5O_{18}]\cdot 1/4(C_2H_5)_2O$ (**C**)

	A	**B**	**C**
Formula	$C_{60}H_{121}N_4O_{18}Mo_5Ti$	$C_{42}H_{88}N_2O_{18}Mo_5Ti$	$C_{27}H_{55.50}NO_{18.25}Mo_5Ti$
Formula weight	1714.21	1436.76	1213.83
T (K)	293(2)	293(2)	93(2)
Crystal system	monoclinic	monoclinic	triclinic
Space group	$P2_1/c$ (no. 14)	$P2_1/n$ (no. 14)	$P\bar{1}$ (no. 2)
a (Å)	12.863(4)	19.9550(4)	12.319(2)
b (Å)	26.608(6)	25.5420(8)	16.105(3)
c (Å)	24.534(4)	11.8820(3)	12.001(2)
α (°)	90	90	110.74(1)
β (°)	103.88(2)	100.31(2)	110.191(3)
γ (°)	90	90	82.777(5)
V (Å^3)	8152(3)	5958.4(4)	2090.0(6)
ρ_{calc} (g cm^{-3})	1.397	1.602	1.929
Z	4	4	2
λ (Å)	0.71069	0.71069	0.71069
μ (mm^{-1})	0.897	1.208	1.702
No. of reflections measured	25 204	10 109	25 119
R_{int}	0.068	0.025	0.118
R [a]	0.070	0.057	0.074
R_w	0.172 [b,c]	0.109 [d]	0.209 [b,e]

[a] $R = \Sigma||F_o|-|F_c||/\Sigma|F_o|$.
[b] $R_w = [\Sigma w(F_o^2-F_c^2)^2/\Sigma w(F_o^2)^2]^{1/2}$ where $w = 1/[\sigma^2(F_o^2)+(aP)^2]$, $P = (F_o^2+2F_c^2)/3$.
[c] $a = 0.0992$.
[d] $R_w = [\Sigma w(|F_o|-|F_c|)^2/\Sigma w(F_o)^2]^{1/2}$ where $w = 1/[\sigma^2(F_o)+F_o^2(P/4)]$, $P = 0.1320$.
[e] $a = 0.0500$.

The higher basicity has lead to a facile synthesis and isolation of two new organometallic derivatives, which will be discussed below.

The monoprotonated species of $[Cp^*TiMo_5O_{18}]^{3-}$ is obtained directly from the reaction of $[(n\text{-}C_4H_9)_4N][Mo_2O_7]$ and Cp^*TiCl_3 in acetone according to Eq. (2).

$$5[Mo_2O_7]^{2-} + 2Cp^*TiCl_3 + H_2O \rightarrow 2[HCp^*TiMo_5O_{18}]^{2-} + 6Cl^- \quad (2)$$

Diprotonation is accomplished by the protonation of $[HCp^*TiMo_5O_{18}]^{2-}$ by CCl_3COOH in $CHCl_3$. The formation of mono- and diprotonated species of $[Cp^*TiMo_5O_{18}]^{3-}$ is confirmed by elemental analysis, IR spectra, and ^1H and ^{17}O NMR spectroscopic data as well as X-ray diffraction studies.

3.2. Solid state structures

X-ray structural analysis revealed that the single crystals of $[(n\text{-}C_4H_9)_4N]_3[Cp^*TiMo_5O_{18}]\cdot CH_3CN$ are composed of $[(n\text{-}C_4H_9)_4N]^+$ cations, CH_3CN molecules of crystallization, and discrete $[Cp^*TiMo_5O_{18}]^{3-}$ anions (**1**) shown in Fig. 1. The current anion has the same basic metal–oxygen framework as the Cp analogue as anticipated. The bond distances in both anions are mostly the same (Tables 2 and 3). The metal–oxygen framework has ideally a C_{4v} symmetry, and Scheme 1 shows the C_{4v}-averaged bond lengths in the $TiMo_3O_4$ rings of **1** and the Cp analogue. Systematic bond length alteration observed in the $TiMo_3O_4$ rings of the Cp compound is also clearly observable in **1**. However, the pattern for the Mo_4O_4 ring is different (see Scheme 2). The Mo_4O_4 ring in **1** does not show the *trans* bond length alteration that resulted in alternating long and short Mo–O bonds along the rings in the Cp analogue and $[Mo_6O_{19}]^{2-}$ [1,15]. Here both of the Mo_2–O_B bonds are significantly shorter than the average Mo–O distance for the Mo_4O_4 ring. Similar loss of the *trans* bond length alternation pattern has been observed in the W_4O_4 ring of $[HCpTiW_5O_{18}]^{2-}$ [6].

One of other noticeable differences is the Mo_5–O_E length. The Mo_5–O_E length in the Cp compound is significantly longer than the other bonds between Mo and terminal oxygen atoms (Mo–O_F). On the other hand, there is no such difference between Mo_5–O_E and Mo–O_F lengths in **1**. Another point in which **1** differs from the Cp analogue is the Ti–O_A length. The Ti–O_A length in **1** is significantly longer than that in the Cp compound. While the O_A atom is slightly displaced from the center of the anion towards the Ti atom in both compounds, it is closer to the center in **1**.

It is interesting to note that solvent molecules are weakly bound on the surface of molecular oxide anions in both cases, possibly by hydrogen bonds. An CH_3CN molecule is attached to the lower half of the anion in **1**

Table 2
Selected interatomic distances (Å) in $[CpTiMo_5O_{18}]^{3-}$ (**Cp**), $[Cp^*TiMo_5O_{18}]^{3-}$ (**1**), $[HCp^*TiMo_5O_{18}]^{2-}$ (**2**), and $[H_2Cp^*TiMo_5O_{18}]^{-}$ (**3**) anions

	Cp [a]	**1**	**2**	**3**
Mo_1–O_A	2.33(2)	2.315(5)	2.333(5)	2.230(9)
Mo_2–O_A	2.32(2)	2.324(5)	2.309(5)	2.323(8)
Mo_3–O_A	2.33(2)	2.311(5)	2.310(5)	2.320(9)
Mo_4–O_A	2.33(2)	2.332(5)	2.302(5)	2.281(8)
Mo_5–O_A	2.42(2)	2.398(5)	2.380(5)	2.291(9)
Mo_1–O_{B1}	1.96(2)	1.951(5)	1.893(5)	1.863(8)
Mo_2–O_{B2}	1.92(2)	1.935(6)	1.910(5)	1.858(9)
Mo_3–O_{B3}	1.90(2)	1.948(7)	1.891(5)	1.887(8)
Mo_4–O_{B4}	1.89(2)	1.948(6)	1.884(6)	1.900(9)
Mo_2–O_{B1}	1.98(2)	1.935(6)	1.979(5)	1.952(9)
Mo_3–O_{B2}	1.98(2)	1.964(7)	1.964(5)	1.946(8)
Mo_4–O_{B3}	1.99(2)	1.962(6)	1.991(6)	1.908(9)
Mo_1–O_{B4}	1.99(2)	1.952(6)	1.970(6)	1.974(8)
Mo_1–O_{C1}	1.97(2)	1.975(5)	2.031(6)	2.099(9)
Mo_2–O_{C2}	1.92(2)	1.968(6)	1.993(5)	2.039(9)
Mo_3–O_{C3}	1.95(2)	1.982(6)	2.062(5)	2.041(9)
Mo_4–O_{C4}	1.95(2)	1.956(6)	2.010(5)	2.093(9)
Mo_5–O_{C1}	1.89(2)	1.892(5)	1.946(6)	2.070(9)
Mo_5–O_{C2}	1.93(2)	1.908(6)	1.858(5)	1.806(8)
Mo_5–O_{C3}	1.91(2)	1.902(6)	1.947(6)	1.789(9)
Mo_5–O_{C4}	1.91(2)	1.913(6)	1.941(6)	2.062(8)
Mo_1–O_{D1}	1.84(2)	1.819(6)	1.832(6)	1.778(9)
Mo_2–O_{D2}	1.80(2)	1.826(6)	1.806(5)	1.791(10)
Mo_3–O_{D3}	1.79(2)	1.802(5)	1.809(5)	1.783(10)
Mo_4–O_{D4}	1.81(2)	1.821(6)	1.841(6)	1.771(9)
Mo_5–O_E	1.73(2)	1.689(6)	1.686(6)	1.677(9)
Mo_1–O_{F1}	1.66(2)	1.715(6)	1.689(6)	1.680(9)
Mo_2–O_{F2}	1.65(2)	1.695(6)	1.686(5)	1.680(9)
Mo_3–O_{F3}	1.65(2)	1.672(6)	1.697(6)	1.680(9)
Mo_4–O_{F4}	1.69(2)	1.707(6)	1.698(6)	1.680(9)
Ti–C_1	2.41(3)	2.419(10)	2.408(9)	2.36(1)
Ti–C_2	2.46(3)	2.406(10)	2.380(8)	2.34(1)
Ti–C_3	2.38(3)	2.432(10)	2.396(9)	2.33(1)
Ti–C_4	2.43(3)	2.444(12)	2.436(10)	2.31(1)
Ti–C_5	2.40(3)	2.462(12)	2.413(9)	2.38(1)
Ti···C_g [b]	2.12(–)	2.13(–)	2.09(–)	2.02(–)
Ti–O_A	2.19(2)	2.247(5)	2.356(5)	2.51(1)
Ti–O_{D1}	1.99(2)	1.980(6)	1.981(6)	1.987(9)
Ti–O_{D2}	2.01(2)	1.988(6)	1.994(5)	1.992(10)
Ti–O_{D3}	2.01(2)	1.990(6)	2.013(5)	1.984(10)
Ti–O_{D4}	1.97(2)	1.980(6)	2.004(6)	1.996(9)
Mo_1···Ti	3.250(5)	3.2517(18)	3.274(2)	3.233(2)
Mo_2···Ti	3.253(5)	3.2665(18)	3.286(2)	3.293(3)
Mo_3···Ti	3.253(5)	3.2448(18)	3.270(2)	3.282(3)
Mo_4···Ti	3.243(6)	3.2566(18)	3.289(2)	3.259(3)
Mo_1···Mo_2	3.284(3)	3.2796(12)	3.2795(9)	3.209(2)
Mo_2···Mo_3	3.299(4)	3.2758(16)	3.2717(9)	3.237(2)
Mo_3···Mo_4	3.285(4)	3.2914(13)	3.263(1)	3.228(2)
Mo_4···Mo_1	3.284(4)	3.2795(15)	3.274(1)	3.236(2)
Mo_5···Mo_1	3.293(6)	3.3031(12)	3.349(1)	3.426(2)
Mo_5···Mo_2	3.305(4)	3.3127(13)	3.2991(9)	3.246(2)
Mo_5···Mo_3	3.297(4)	3.3122(13)	3.372(1)	3.254(2)
Mo_5···Mo_4	3.293(3)	3.3171(13)	3.346(1)	3.471(2)

The numbers in parentheses are the estimated S.D.s in the last significant digits.

[a] Ref. [1].

[b] C_g is used to denote the center-of-gravity for the five carbons forming the ring.

Table 3
C_{4v}-averaged interatomic distances (Å) in $[CpTiMo_5O_{18}]^{3-}$ (**Cp**), $[Cp^*TiMo_5O_{18}]^{3-}$ (**1**), $[HCp^*TiMo_5O_{18}]^{2-}$ (**2**), and $[H_2Cp^*TiMo_5O_{18}]^{-}$ (**3**) anions

	Cp [a]	**1**	**2**	**3**
Mo_e [b]–O_A	2.33	2.321	2.314	2.29
Mo_5–O_A	2.42	2.398	2.380	2.291
Mo_e [b]–O_B	1.95	1.949	1.935	1.91
Mo_e [b]–O_C	1.95	1.970	2.024	2.07
Mo_5–O_C	1.91	1.904	1.923	1.93
Mo_e [b]–O_D	1.81	1.817	1.822	1.78
Mo_5–O_E	1.73	1.689	1.686	1.677
Mo_e [b]–O_F	1.66	1.697	1.693	1.68
Ti–C [c]	2.42	2.43	2.41	2.34
Ti–C_g [d]	2.12	2.13	2.09	2.02
Ti–O_A	2.19	2.247	2.356	2.51
Ti–O_D	2.00	1.985	1.998	1.99
Mo_e [b]···Ti	3.250	3.255	3.280	3.267
Mo_5···Ti	4.607	4.645	4.735	4.788
Mo_e···Mo_e [b]	3.288	3.282	3.272	3.228
Mo_5···Mo_e [b]	3.297	3.311	3.342	3.349

[a] Ref. [1].

[b] Mo_e denotes for the four Mo atoms on the 'equator' of the anion; Mo_1, Mo_2, Mo_3, and Mo_4.

[c] Average of five Ti–C bonds.

[d] C_g is used to denote the center-of-gravity for the five carbons forming the ring.

(C···O_{B2} 3.15 Å, C···O_{C2} 3.05 Å), while a CH_2Cl_2 molecule is attached to the upper half of the anion in the Cp analogue (C···O_{D1} 3.16 Å, C···O_{D4} 3.34 Å, C···O_{B4} 2.95 Å). The different positions of the solvent molecules may be the consequence of the difference of the steric repulsion and/or the different location of the most basic oxygen atoms. This point will be further discussed later.

Fig. 2 shows the structure of the $[HCp^*TiMo_5O_{18}]^{2-}$ anion (**2**). Although the acidic proton was not located by X-ray diffraction, its location can be reasonably inferred

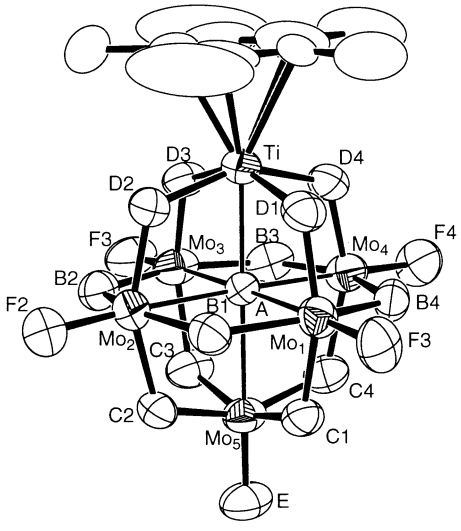

Fig. 1. Perspective drawing of **1**. Displacement ellipsoids are scaled to enclose 50% probability levels. Oxygen atoms are labeled by their subscripts only.

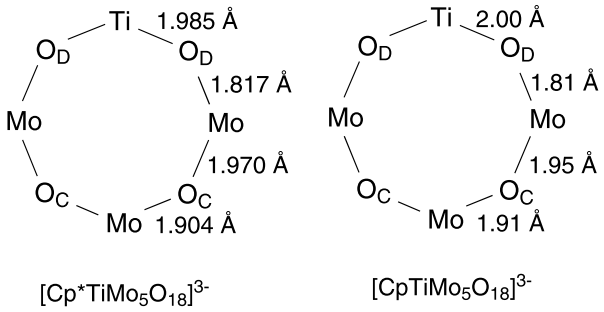

Scheme 1.

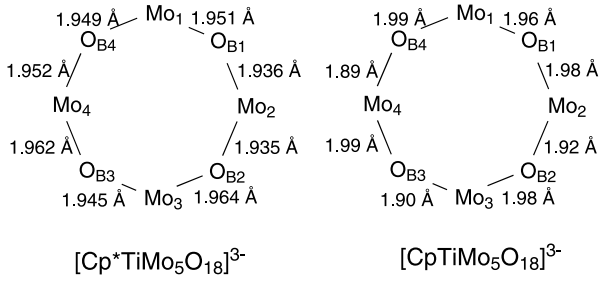

Scheme 2.

from a comparison of bond lengths in anions **1** and **2** and bond valence calculations [16]. The Mo–O bonds involving O_{C1}, O_{C3}, and O_{C4} atoms are anomalously long and the apparent valences of these oxygen atoms are anomalously small: 1.6 for O_{C1} and O_{C3}, 1.7 for O_{C4}. This suggests that the proton is attached to one of these O_C oxygen atoms. Interestingly, the Mo_4O_4 ring of **2**

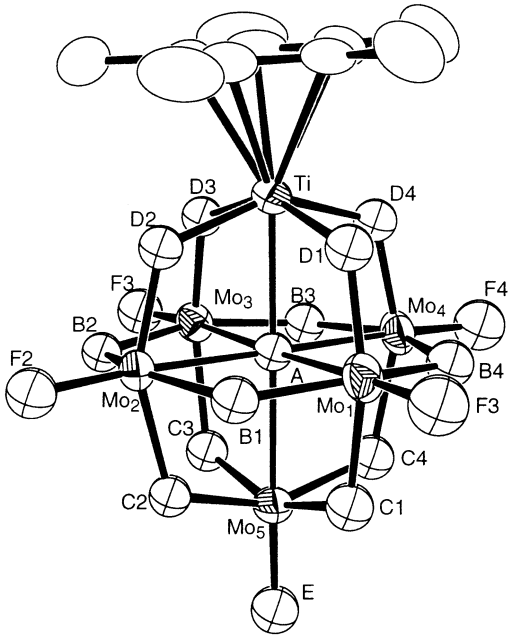

Fig. 2. Perspective drawing of **2**. Displacement ellipsoids are scaled to enclose 50% probability levels. Oxygen atoms are labeled by their subscripts only.

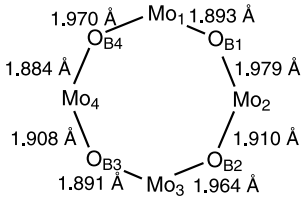

Scheme 3.

clearly shows a *trans* bond length alternation unlike its conjugate base, **1** (see Scheme 3).

Fig. 3 shows the structure of the diprotonated anion, $[H_2Cp^*TiMo_5O_{18}]^-$ (**3**). As was the case for anion **2**, the acidic protons in $[H_2Cp^*TiMo_5O_{18}]^-$ could not be located X-ray crystallographically. Their locations could be inferred, however, by comparison of bond length in anions **1** and **3** and bond valence calculations. The bonds to oxygens O_{C1} and O_{C4} are unusually long and the apparent valences of these oxygens are anomalously small: 1.2 for O_{C1} and 1.3 for O_{C4}. This identifies these oxygen atoms as the protonation sites.

The $[H_2Cp^*TiMo_5O_{18}]$ anions are present in the lattice as hydrogen-bonded dimers (Fig. 4). Two pairs of short contacts ($O_{C1}\cdots O_{B4}$ 2.71 Å, $O_{C4}\cdots O_{F1}$ 2.64 Å) strongly suggest hydrogen bonding. These hydrogen bonds unite two anions to make an extended array of close-packed oxygens. The hydrogen-bonded dimer can also be viewed as a molecular lamellar intercalation complex where four protons are intercalated between the planar faces of two $[Cp^*TiMo_5O_{18}]^{3-}$ anions. Similar molecular lamellar structure has been observed for $[H_3V_{10}O_{28}]^{3-}$ [17].

X-ray structural analyses revealed that oxygen atoms bridging two Mo atoms (O_C oxygens) are protonated in both **2** and **3**. This was totally unexpected and is in marked contrast with the results obtained for $[HCpTiW_5O_{18}]^{2-}$ and $[H_2CpTiW_5O_{18}]^-$, where the protons are attached to those oxygen atoms that connect Ti and W (O_D oxygens). Simple electrostatic argument would predict O_D oxygens most basic. The current results strongly suggest that the large steric bulk of Cp* is making O_D oxygens inaccessible even to a very small cation like H^+ and thus effectively making O_C oxygens the most basic sites.

Nonlocal effects of protonation are also apparent in Tables 2 and 3. The average distance between O_A and four Mo atoms on the 'equator' of the anion (Mo_1, Mo_2, Mo_3, and Mo_4, collectively referred to as Mo_e hereafter) decrease systematically with protonation. The Mo_e–O_B and $Mo_e\cdots Mo_e$ distances also show similar decreasing trend. On the other hand, Mo_e–O_C, Mo_5–O_C, and $Mo_5\cdots Mo_e$ distances all increase with protonation as well as the $Ti\cdots Mo_5$ distance. In other words, protonation makes the $[Cp^*TiMo_5O_{18}]^{3-}$ anion more 'skinny' and 'taller'.

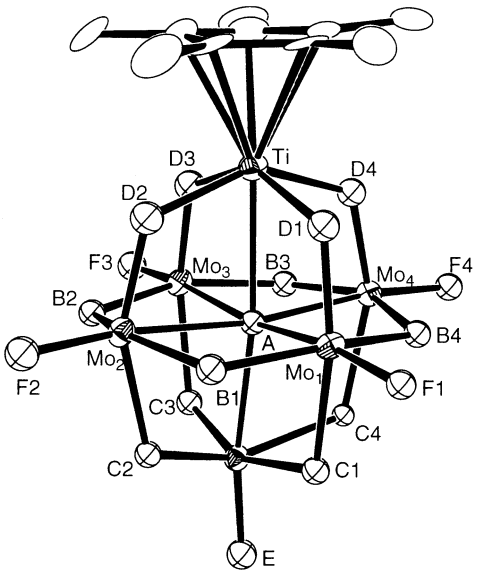

Fig. 3. Perspective drawing of **3**. Displacement ellipsoids are scaled to enclose 50% probability levels. Oxygen atoms are labeled by their subscripts only.

Protonation also affects the position of O_A in the anion in an interesting manner. In the unprotonated anion **1**, O_A is located slightly above the equatorial plane defined by four Mo_e atoms. It shifts towards Mo_5 on protonation and it is definitely below the equatorial plane in the diprotonated **3**. The Mo_5–O_A distance decreases and the Ti–O_A increases with protonation. This observation can be interpreted in terms of charge compensation. In the current compound, protonation takes place on O_C oxygens and reduces the local charge of the bottom half of the anion. The O_A atom, which is strongly anionic in character, shifts itself towards Mo_5 to compensate the charge decrease. This in turn leads to a lengthening of the Ti–O_A bond. Since the Ti–O_D bonds do not change significantly on protonation, constant valence at Ti can be approximated only if the Ti–Cp* bond is strengthened. This is in fact the case. The distance between the Ti atom and Cp* ring decreases with increasing degree of protonation.

In $[CpTiW_5O_{18}]^{3-}$, on the other hand, the Ti–O_A bond shortens and Mo_5–O_A bond lengthens on protonation [6]. This seemingly contradicting observation can be explained by the same charge compensation theory. Here the protonation occurs at O_D oxygens and the local charge of the upper half is decreased on protonation. This is compensated by moving O_A towards the Ti atom, making the Ti–O_A bond shorter and the Mo_5–O_A bond longer.

3.3. Reaction of $[Cp^*TiMo_5O_{18}]^{3-}$ with organometallic cations

The anion **1** reacts readily with organometallic cations like $[(\eta\text{-}C_8H_{12})Ir]^+$ and $[(\eta\text{-}C_8H_{14})Rh]^+$ to form polyoxoanion-supported organometallic compounds in high yields.

$$[Cp^*TiMo_5O_{18}]^{3-} + [(\eta\text{-}C_8H_{12})Ir]^+ \rightarrow [(\eta\text{-}C_8H_{12})Ir(Cp^*TiMo_5O_{18})]^{2-} \quad (3)$$

$$[Cp^*TiMo_5O_{18}]^{3-} + [(\eta\text{-}C_8H_{14})Rh]^+ \rightarrow [(\eta\text{-}C_8H_{14})Rh(Cp^*TiMo_5O_{18})]^{2-} \quad (4)$$

These results confirm the high basicity of **1**. The IR, elemental analysis, and NMR data strongly suggest

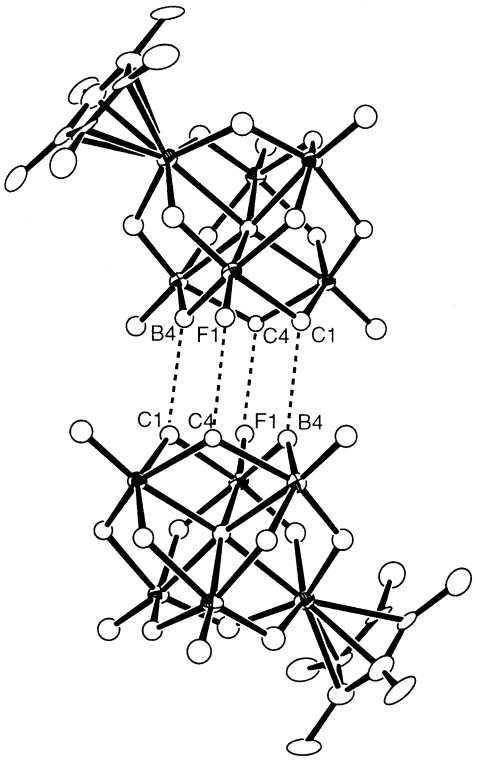

Fig. 4. Perspective drawing of the $[H_2Cp^*TiMo_5O_{18}]_2^{2-}$ dimer found in crystalline $[(n\text{-}C_4H_9)_4N][H_2Cp^*TiMo_5O_{18}]\cdot 1/4(C_2H_5)_2O$.

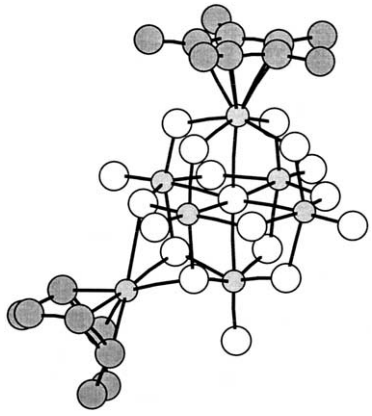

Fig. 5. Perspective drawing of the $[(\eta\text{-}C_8H_{12})Ir(Cp^*TiW_5O_{18})]^{2-}$ anion. Oxygen and carbon atoms are represented by white and dark-shaded spheres, respectively. Metals atoms are represented by small hatched spheres.

these compounds have the same basic structure as $[(\eta\text{-}C_8H_{12})Ir(Cp^*TiW_5O_{18})]^{2-}$ (Fig. 5) [14] although they have not been subjected to X-ray crystallographic study. Attempt to synthesize $[(\eta\text{-}C_4H_7)_2Rh(Cp^*TiMo_5O_{18})]^{2-}$, a methallyl rhodium adduct, by reacting $[(\eta\text{-}C_4H_7)_2Rh]^+$ and **1** was not successful. The reaction in $CHCl_3$ yielded a diene rhodium compound $[(\eta\text{-}C_8H_{14})Rh(Cp^*TiMo_5O_{18})]^{2-}$ instead, which was characterized by IR and NMR (^1H and ^{17}O). No reaction proceeded in CH_3CN and CH_2Cl_2.

4. Supplementary material

X-ray data for the structural analysis have been deposited with the Cambridge Crystallographic Data Centre, CCDC Nos. 170157–170159. Copies of this information may be obtained free of charge from The Director, CCDC, 12 Union Road, Cambridge, CB2 1EZ, UK (fax: +44-1223-336033; e-mail: deposit@ccdc.cam.ac.uk or www: http://www.ccdc.cam.ac.uk).

Acknowledgements

This work was supported in part by Grants-in-Aid No. 13640555 from MEXT of Japan (Monbukagakusho).

References

[1] T.M. Che, V.W. Day, L.C. Francesconi, M.F. Frecrich, W.G. Klemperer, Inorg. Chem. 24 (1985) 4055.
[2] C.J. Besecker, V.W. Day, W.G. Klemperer, M.R. Thompson, Inorg. Chem. 24 (1985) 44.
[3] M. Pohl, Y.L.T.J.R. Weakley, K. Nomiya, M. Kaneko, H. Weiner, R.G. Finke, Inorg. Chem. 34 (1995) 767.
[4] D.J. Edlund, R.J. Saxton, D.K. Lyon, R.G. Finke, Organometallics 7 (1988) 1692.
[5] P. Gouzerh, A. Proust, Chem. Rev. 98 (1998) 77.
[6] T.M. Che, V.W. Day, L.C. Francesconi, W.G. Klemperer, D.J. Main, A. Yagasaki, O.M. Yaghi, Inorg. Chem. 31 (1992) 2920.
[7] V.W. Day, M.F. Fredrich, M.R. Thompson, W.G. Klemperer, R.-S. Liu, W. Shum, J. Am. Chem. Soc. 103 (1981) 3597.
[8] H. Akashi, J. Chen, T. Sakuraba, A. Yagasaki, Polyhedron 13 (1994) 1091.
[9] N.H. Hur, W.G. Klemperer, R.-C. Wang, Inorg. Synth. 27 (1990) 79.
[10] A.C. Sievert, E.L. Muetterties, Inorg. Chem. 20 (1981) 489.
[11] Peaks for the $(\eta\text{-}C_8H_{14})Rh$ group overlap severely with those of the cation.
[12] TEXSAN, crystal structure analysis package, Molecular Structure Corporation, The Woodlands, TX, USA, 1999.
[13] G.M. Sheldrick, SHELX-97, Program for the Analysis of Crystal Structures, University of Göttingen, Germany, 1997.
[14] W.G. Klemperer, A. Yagasaki, Chem. Lett. (1989) 2041.
[15] H.R. Allcock, E.C. Bissell, E.T. Shawl, Inorg. Chem. 12 (1973) 2963.
[16] I.D. Brown, D. Altermatt, Acta Crystallogr., Sect. B B41 (1985) 244.
[17] V.W. Day, W.G. Klemperer, D.J. Maltbie, J. Am. Chem. Soc. 109 (1987) 2991.